

Imaging mass spectrometry reveals co-accumulation of aldosterone and 18-oxocortisol with CYP11B2 in pre-adrenomatous states of primary aldosteronism

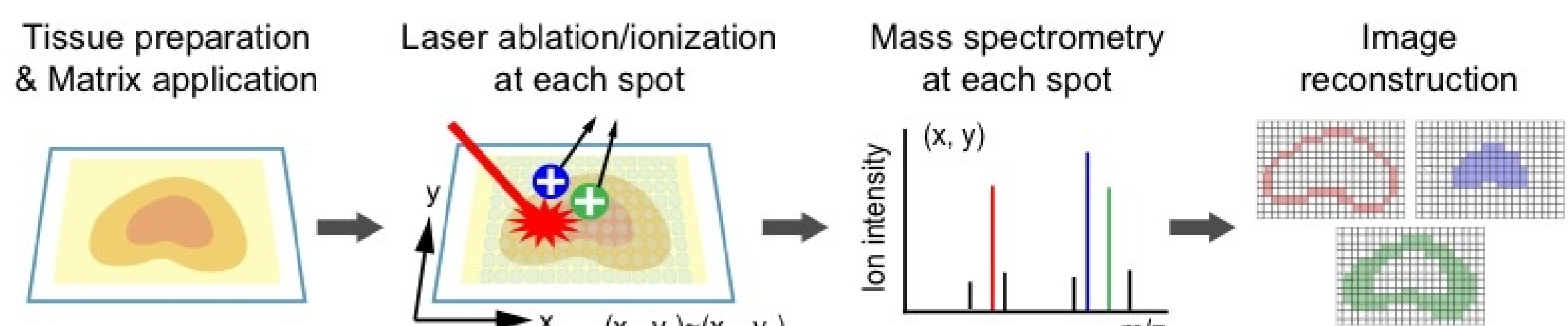
Yuki Sugiura¹, Emi Takeo², Shuichi Shimma², Mai Yokota³, Tatsuya Higashi³, Tsuguo Seki⁴, Yosuke Mizuno⁵, Mototsugu Oya⁶, Takeo Kosaka⁶, Masao Omura⁷, Tetsuo Nishikawa⁷, Makoto Suematsu¹, **Koshiro Nishimoto^{1,8}**
¹Department of Biochemistry, Keio University School of Medicine, Tokyo 160-8582, Japan; ²Department of Biotechnology, Graduate School of Engineering, Osaka University, Osaka 565-0871, Japan; ³Faculty of Pharmaceutical Sciences, Tokyo University of Science, Noda, Chiba 278-8510, Japan; ⁴Department of Medical Education, School of Medicine, California University of Science and Medicine, San Bernardino, CA 92408, USA; ⁵Division of Functional Genomics & Systems Medicine, Research Center for Genomic Medicine, Saitama Medical University, Hidaka-shi, Saitama, Japan; ⁶Department of Urology, Keio University School of Medicine, Tokyo 160-8582, Japan; ⁷Endocrinology and Diabetes Center, Yokohama Rosai Hospital, Yokohama 222-0036, Japan; ⁸Department of Uro-Oncology, Saitama Medical University International Medical Center, Hidaka 350-1241, Japan

Abstract

Primary aldosteronism (PA) is a secondary hypertensive disease caused by autonomous aldosterone production that often caused by aldosterone-producing adenoma (APA). Immunohistochemistry of aldosterone synthase (CYP11B2) shows the presence of aldosterone-producing cell clusters (APCCs) even in non-PA adult adrenal cortex (Ref. 1,2). An APCC-like portion also exists in possible APCC-to-APA transitional regions (pAATLs) in PA adrenals (Ref. 3). However, whether APCCs produce aldosterone or 18-oxocortisol (18-oxoF), a serum marker of APA, remains unknown due to lack of technology to visualize adrenocorticosteroids on tissue sections. In the present study, we utilized highly sensitive Fourier transform ion cyclotron resonance mass spectrometry to image various adrenocorticosteroids, including 18-oxoF, in adrenal tissue sections from 8 PA patients with APCC (Cases 1-4), pAATL (Case 5), and APA (Cases 6-8). Further analyses by tandem mass spectrometry imaging allowed us to differentially visualize aldosterone from cortisone, which share identical *m/z*. These advanced imaging techniques revealed that aldosterone and 18-oxoF co-accumulated within CYP11B2-expressing lesions. These imaging outcomes along with a growing body of aldosterone research led us to build a progressive development hypothesis of an aldosterone-producing pathology in the adrenal glands.

Patients and methods

MALDI-IMS: Matrix-Assisted Laser Desorption/Ionization-Imaging Mass Spectrometry



Chemical derivatization using GirT reagent

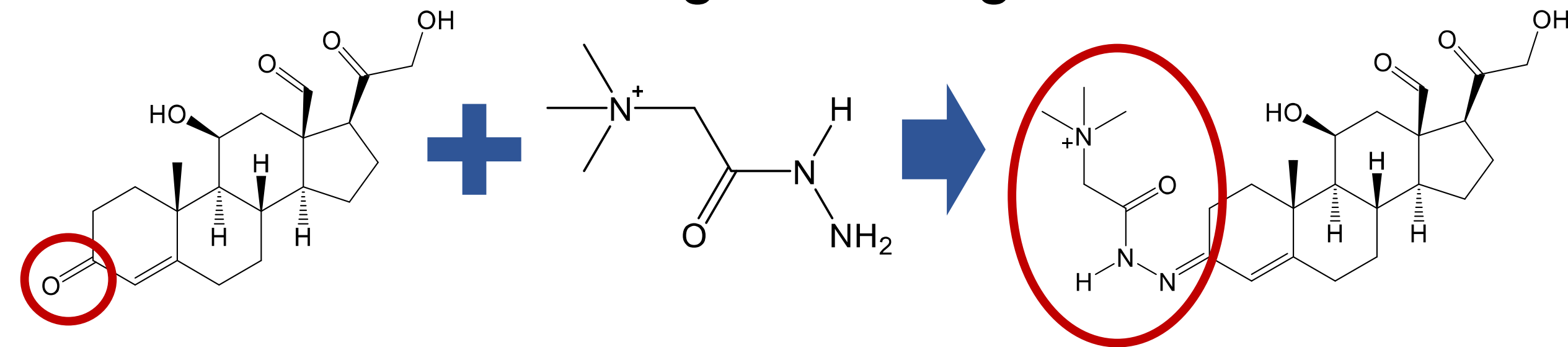


Table 1. Clinical data and steroid concentrations of adrenal tissue sections.

Case#	YRPA#	Age (year)	Sex	SAC after saline infusion*	Computed tomography (Supplemental Figure 1)	Lateralized ratio of CAVS with ACTH loading	Surgery	Section area (mm ²)	Steroid amount (picogram [pg] per section and pg per area [pg/mm ²], in parentheses)***			
									aldosterone	cortisone	18-oxoF	
APCC	1	7927	30	male	96	normal	3.0	right total adx	57.1	129.0 ± 8.0 (2.26 ± 0.14)	251.9 ± 21.7 (4.41 ± 0.38)	26.9 ± 1.8 (0.47 ± 0.03)
	2	1157	50	male	118	left adenoma	3.2	right total adx	90.5	<45.2 (-0.50)	588.4 ± 13.2 (6.50 ± 0.15)	11.1 ± 1.4 (0.12 ± 0.02)
	3	7943	60	female	65	left adenoma	1.2	left partial adx	41.2	46.6 ± 0.6 (1.13 ± 0.02)	91.1 ± 4.7 (2.21 ± 0.11)	13.2 ± 1.2 (0.32 ± 0.03)
	4	6882	49	male	66	right multiple nodules	2.6	right total adx	36.9	<45.2 (-1.22)	64.6 ± 3.4 (1.75 ± 0.09)	<8.5 (-0.23)
APA (including pAATL #6)	5	7893	47	male	408	left adenoma	26.3	left partial adx	108.8	380.4 ± 5.9 (3.50 ± 0.04)	668.9 ± 4.0 (6.14 ± 0.04)	228.3 ± 5.6 (2.10 ± 0.05)
	6	7841	60	male	149	right adenoma	5.5	right partial adx	32.2	325.4 ± 18.3 (10.10 ± 0.57)	225.9 ± 18.4 (7.02 ± 0.57)	89.4 ± 6.8 (2.78 ± 0.21)
	7	7626	55	male	120	right adenoma	1.4 (99.6)**	right partial adx	76.9	3460.3 ± 154.7 (45.00 ± 2.01)	91.0 ± 6.9 (1.18 ± 0.09)	245.4 ± 5.4 (3.19 ± 0.07)
	8	6303	46	female	779	left adenoma	23.7	left partial adx	98.1	110.0 ± 13.1 (1.12 ± 0.13)	69.6 ± 6.5 (0.71 ± 0.07)	70.8 ± 6.6 (0.7 ± 0.1)
average ± standard error or median [interquartile range] of the concentration per area (nm ²)								APCC	0.87 (0.34 - 1.98)	3.72 ± 1.09	0.26 ± 0.09	
								APA	7.97 (2.30 - 36.27)	4.80 ± 2.33	2.20 ± 0.54	
								p value	0.114*	0.983**	0.0122**	

SAC: serum aldosterone concentration, APCC: aldosterone-producing cell cluster, APA: aldosterone-producing adenoma, pAATL: possible APCC-to-APA transitional lesion, CAVS: conventional adrenal venous sampling, ACTH: adrenocorticotropic hormone, 18-oxoF: 18-oxocortisol, YRPA#: a unique non-sequential control number for patients with PA in Yokohama Rosai Hospital, *: saline infusion test (SAC levels after saline infusion <50 pg/mL make the diagnosis of primary aldosteronism (PA) unlikely, and levels >100 pg/mL are a very probable sign of PA. Values between 50 and 100 pg/mL are indeterminate. Funder et al. J Clin Endocrinol Metab 2008;93:3266-81. **): lateralized ratio of CAVS without ACTH loading. ***): average ± standard error values of four sections (see Supplemental Table 2). #: Mann-Whitney Rank Sum Test, #: The Student's *t*-test.

Results

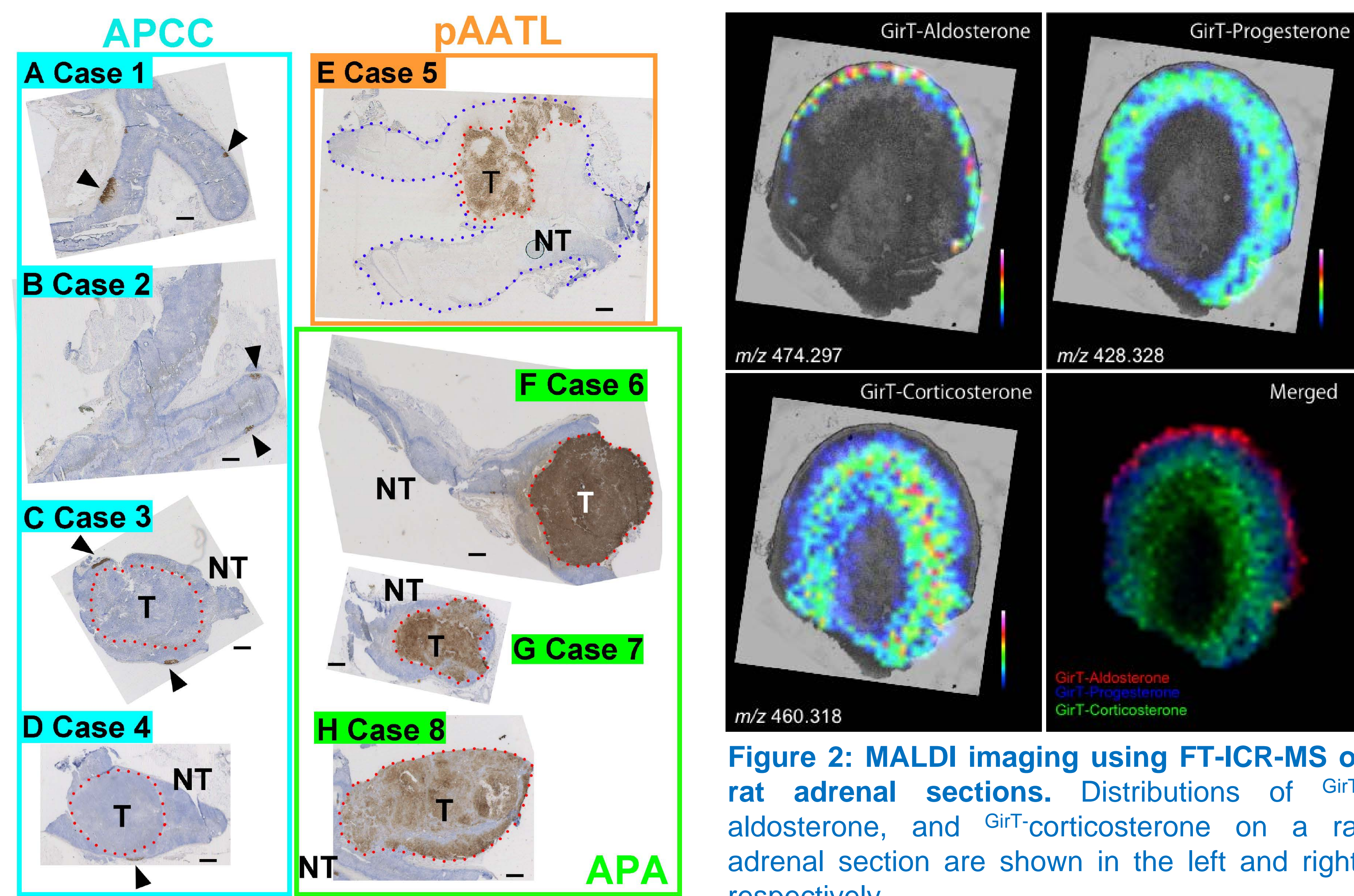


Figure 1: Immunohistochemistry for CYP11B2 in human adrenalectomized samples. Panels (A–D), (E), and (F–H) show immunohistochemistry for samples of APCCs (arrowheads), pAATL, and APA, respectively. In (C–H), areas marked with red dotted lines indicate a tumor (T); outside of these areas constitutes the adjacent normal adrenal tissue (non-tumor portion: NT). Tumors in (C–D) and (E–H) are non-functional adenoma and APA, respectively. All panels are shown at the same magnification. Bars indicate 1 mm. Case numbers marked by blue, orange, and green indicate cases of APCC (cases 1–4), pAATL (case 5), and APA (cases 6–8), respectively.

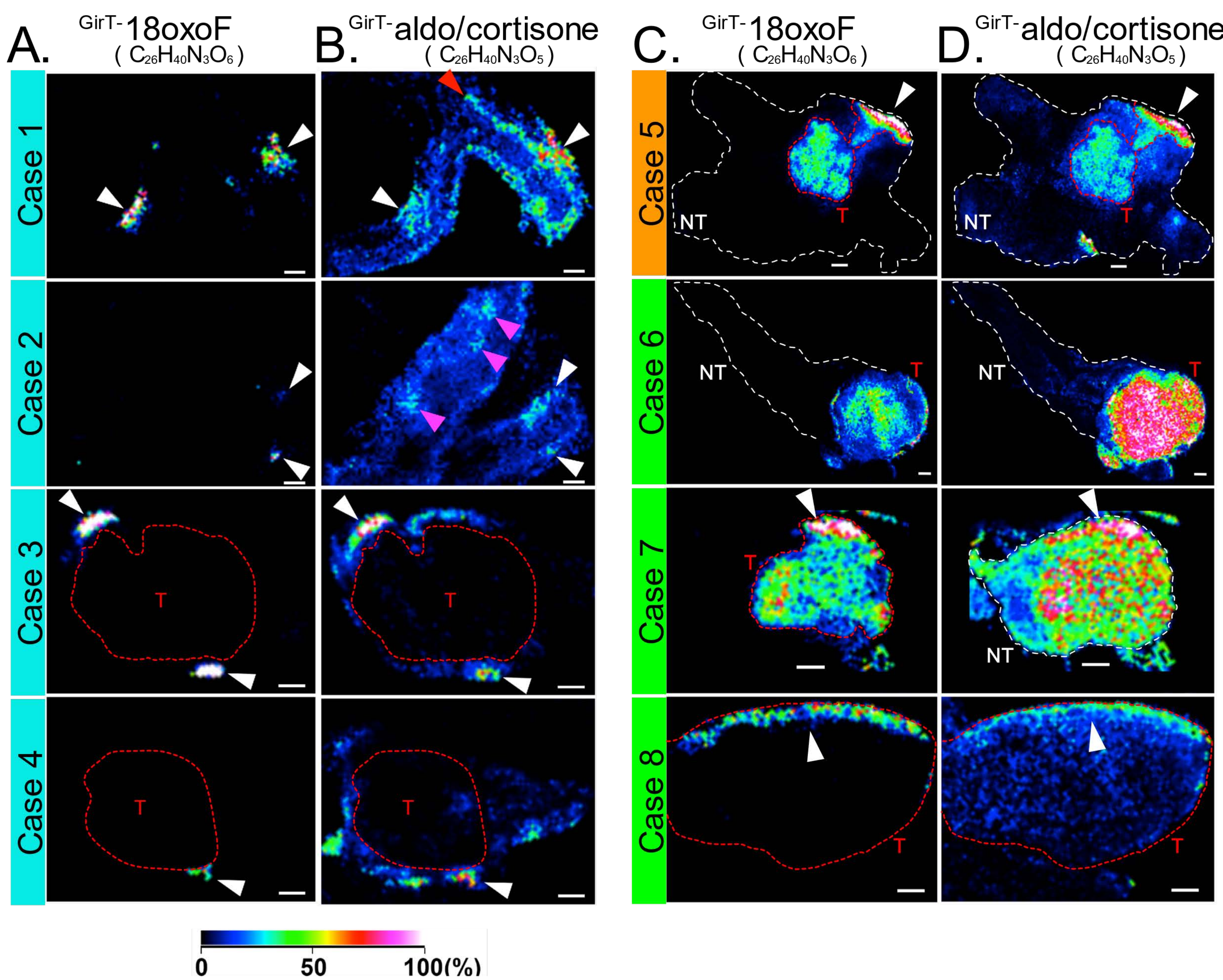


Figure 2: MALDI imaging using FT-ICR-MS of rat adrenal sections. Distributions of *GirT*-aldosterone, *GirT*-progesterone, *GirT*-corticosterone, and *GirT*-corticosterone on a rat adrenal section are shown in the left and right, respectively. Figure 3: MALDI imaging of APCC, pAATL, and APA using FT-IMS-MS (a–p). Case numbers marked by blue, orange, and green indicate cases of APCC (Cases 1–4), pAATL (Case 5), and APA (Cases 6–8), respectively. In MALDI imaging using FT-IMS-MS, the signals of the derivatized steroids, *GirT*-aldosterone and *GirT*-cortisone (*GirT*-aldo/cortisone) as well as that of *GirT*-18-oxoF are shown on a single section from each case. White arrowheads in panels (a–h) correspond to APCCs in Figure 1A–1D. Tumor (marked by "T" and the orange dotted line) and non-tumor portions (marked by the white dotted line in Cases 5–7) of imaging sections correspond to those of CYP11B2 immunohistochemistry in Figure 1. Bars indicate 1 mm.

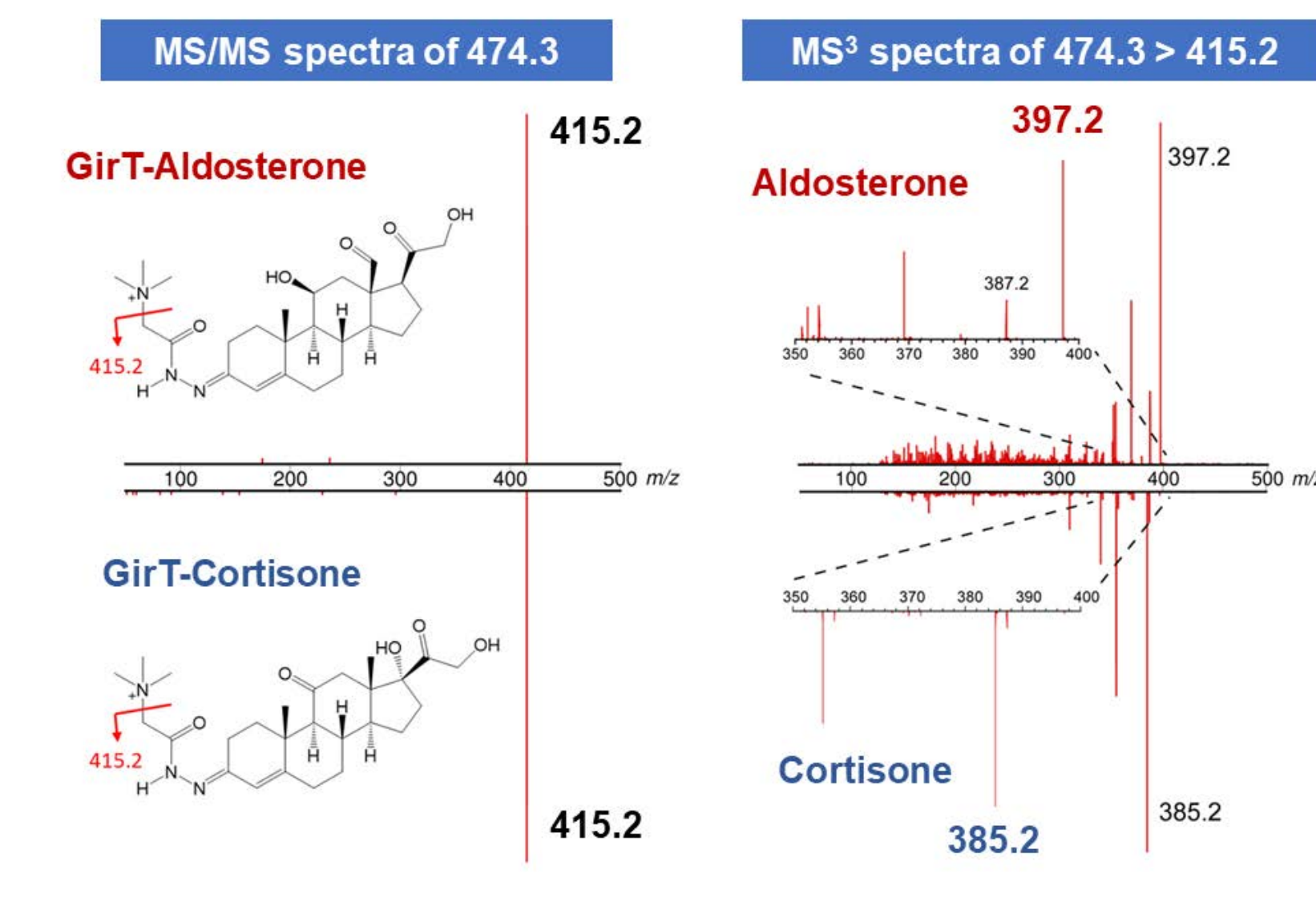


Figure 4: Discrimination of aldosterone from cortisone, an isomer of aldosterone. In order to differentiate the aldosterone-specific signal from the cortisone-derived signal on adrenal sections, we further established a tandem-MS imaging method with a linear ion trap-type instrument. An initial attempt using the tandem MS method (*MS*²) revealed that derivatized aldosterone and cortisone still showed the same ion transition, i.e., from *m/z* 474.3 to 415.2, representing a common dissociation reaction of the *GirT* moiety. However, one additional tandem MS (*MS*³) enabled the differentiation of distinct steroid structures and gave independent signals for aldosterone and cortisone; i.e., *m/z* 474.3 > 415.2 > 397.2 and *m/z* 474.2 > 415.2 > 385.2, respectively.

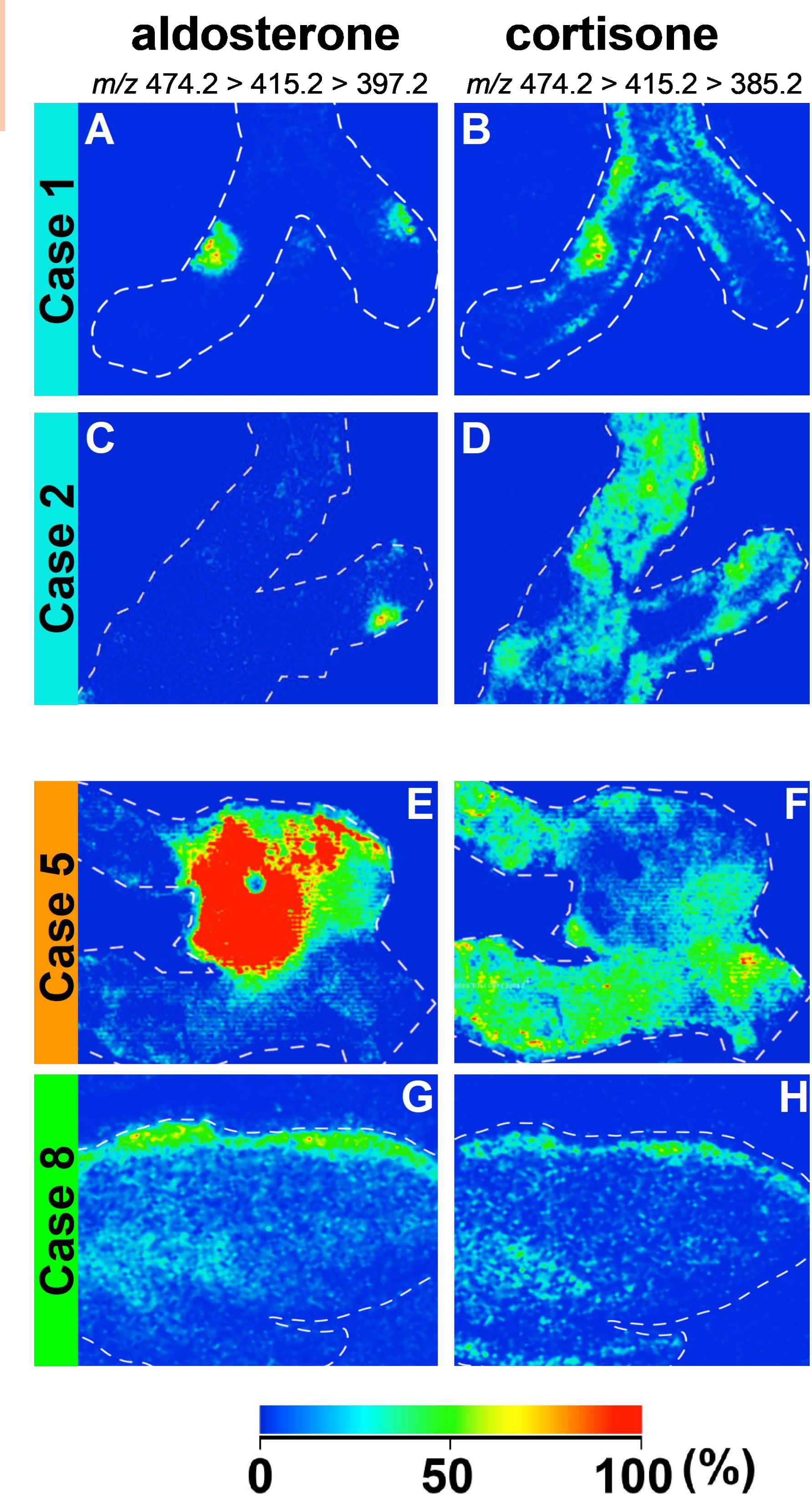


Figure 5: MALDI imaging of APCC, pAATL, and APA using tandem-MS (*MS*³). Case numbers marked by blue, orange, and green indicate cases of APCC (cases 1–2), pAATL (case 5), and APA (cases 8), respectively. The signals of the derivatized steroids, *GirT*-aldosterone (left) and *GirT*-cortisone (right) are shown on a single section of each case.

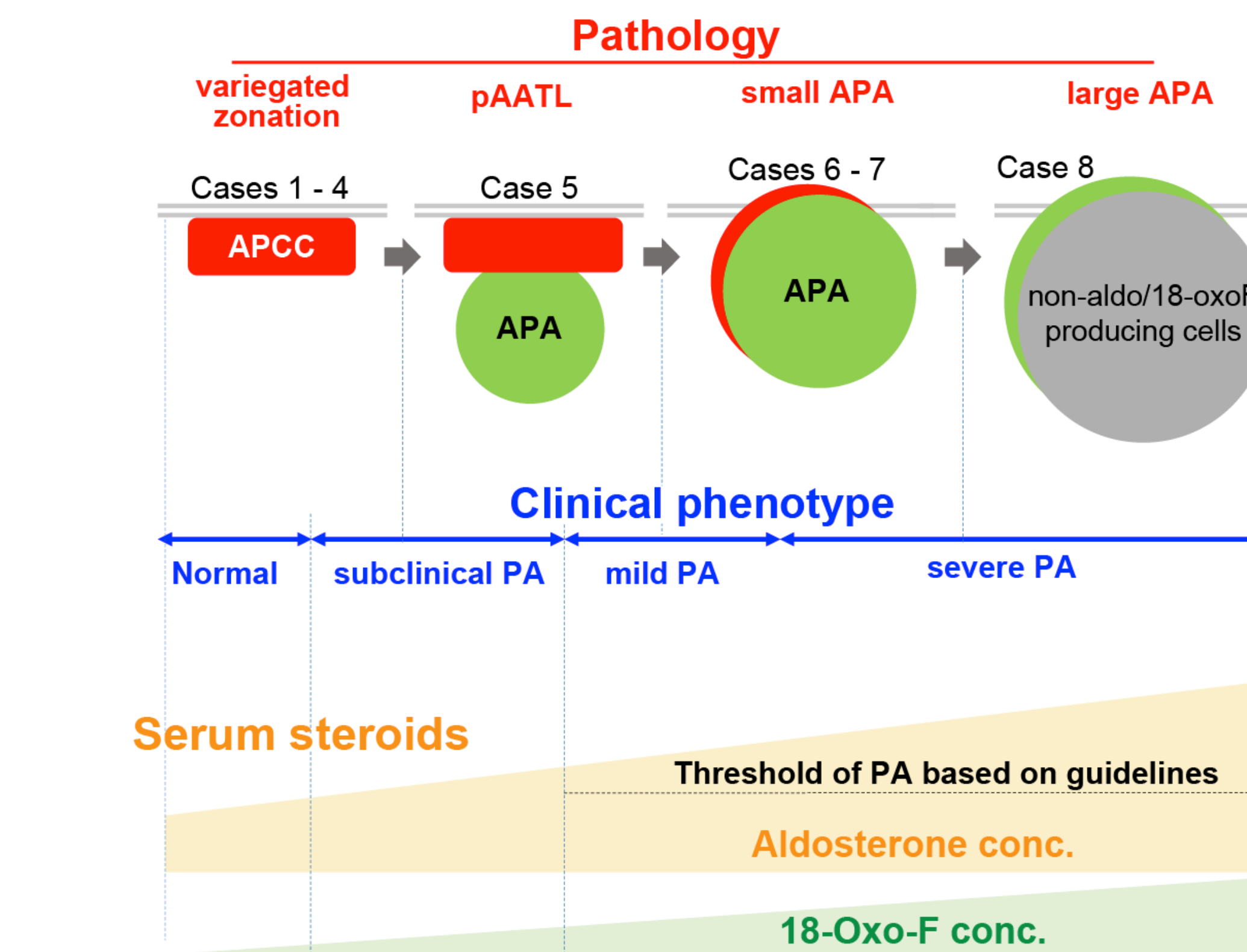


Figure 5: Schematic showing APA generation and its clinical significance. Pathologies supporting our hypothesis that APCC develops into APA via a possible APCC-to-APA transitional lesion (pAATL). pAATL consists of a sub-capsular APCC-like region and inner APA-like region. The APCC and APCC-like regions of pAATL consist of aldosterone-producing cells, whereas the APA-like region of pAATL and small APA contain aldosterone- and cortisol-producing cells. Large APA consists of aldosterone synthase (CYP11B2)-positive aldosterone-producing areas and

CYP11B2-positive non-functional areas, with the latter potentially lacking precursor steroids, including progesterone. Putative phenotypes and serum aldosterone and 18-oxoF concentrations are indicated at the bottom along with the thresholds for subclinical and clinical PA.

Conclusions

Steroid imaging by MALDI-IMS revealed heterogeneous steroid localization patterns provided insight into the spatio-temporal relationship between altered steroid hormone production and a cell lineage leading toward primary aldosteronism lesions.

References

- Nishimoto, K. *et al.* Adrenocortical zonation in humans under normal and pathological conditions. *J Clin Endocrinol Metab* **95**, 2296-305 (2010).
- Nishimoto, K. *et al.* Aldosterone-stimulating somatic gene mutations are common in normal adrenal glands. *Proc Natl Acad Sci U S A* **112**, E4591-9 (2015).
- Nishimoto, K. *et al.* Case Report: Nodule Development From Subcapsular Aldosterone-Producing Cell Clusters Causes Hyperaldosteronism. *J Clin Endocrinol Metab* **101**, 6-9 (2016).